Electronic Supplementary Material (ESI) for Journal of Materials Chemistry A.

A coaxial zinc-tin vertically oriented arrays anode achieving ultrahigh areal current and capacity up-to 80 mA cm^{-2} and 80 mAh cm^{-2}

Shiwen Wang, Huaiyang Zheng, Junwei Ding*, Shide Wu, and Shaoming Fang*

Henan Provincial Key Laboratory of Surface & Interface Science and College of Materials and Chemical Engineering, Zhengzhou University of Light Industry, Zhengzhou 450002, China.
Email: dingjunwei@zzuli.edu.cn, mingfang@zzuli.edu.cn.

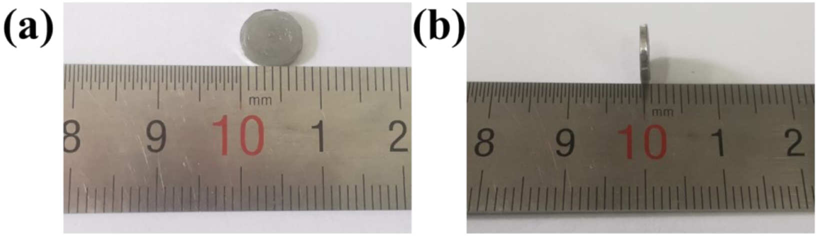

Figure S1. Optical images of the obtained Zn-Sn vertical arrays with (a) the diameter of about 7.5 mm and (b) the thickness of about 1000 μm.

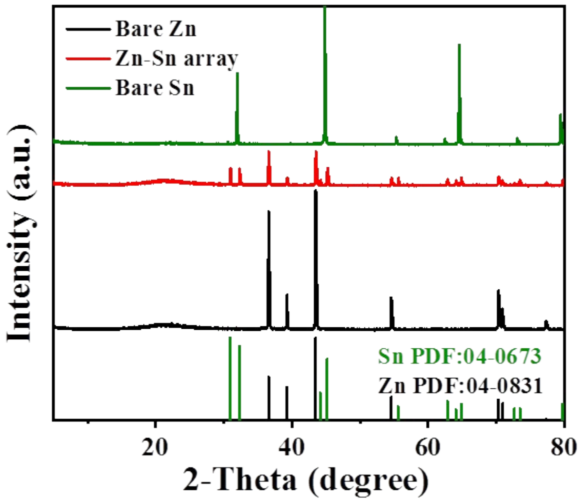

Figure S2. XRD patterns of bare Zn foil, bare Sn foil, and the obtained Zn-Sn vertical arrays.

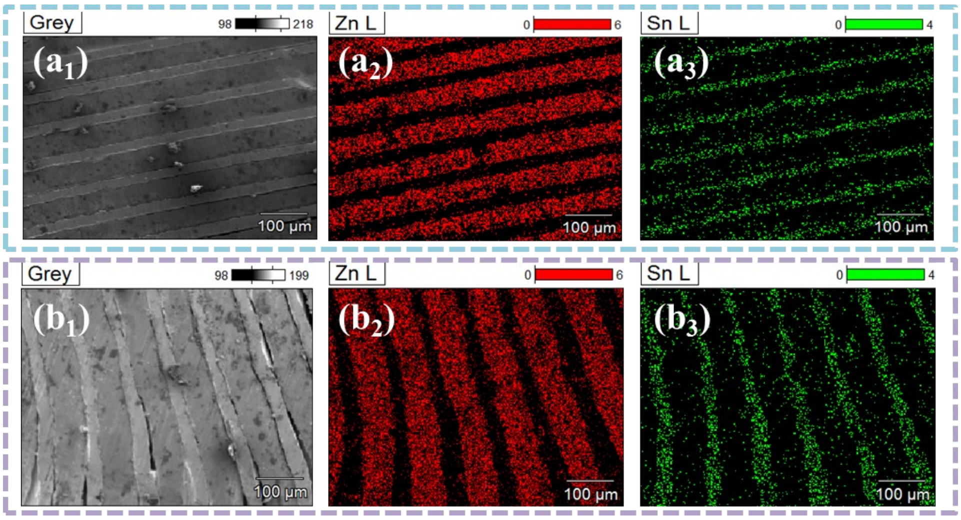

Figure S3. The SEM and corresponding mapping images of the Zn-Sn vertical arrays anode of (a$_1$-a$_3$) 40 μm Zn-20 μm Sn and (b$_1$-b$_3$) 80 μm Zn-20 μm Sn.

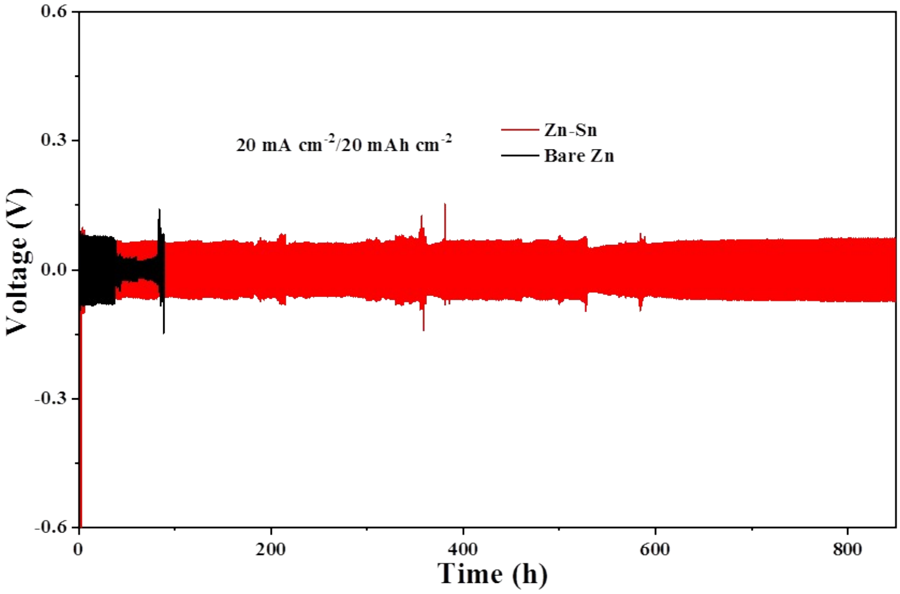

Figure S4. Cycle performance at 20 mA cm^{-2}/20 mAh cm^{-2} of the Zn-Sn vertically oriented arrays and bare Zn based symmetrical cells.

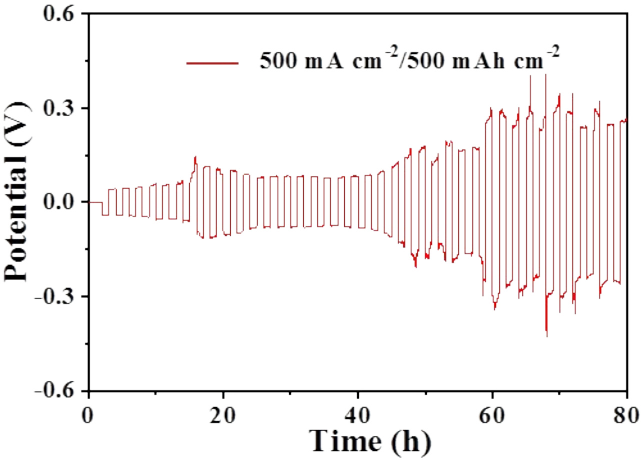

Figure S5. Cycle performance at 500 mA cm^{-2}/500 mAh cm^{-2} of the Zn-Sn vertically oriented arrays based symmetrical cells.

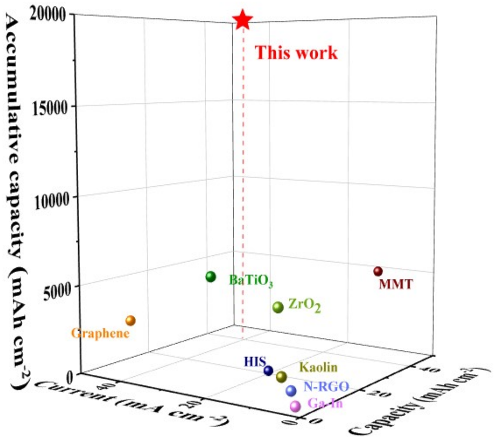

Figure S6. The cumulative plating capacity comparison of the Zn-Sn vertically oriented arrays and zinc anodes with different modification strategies.

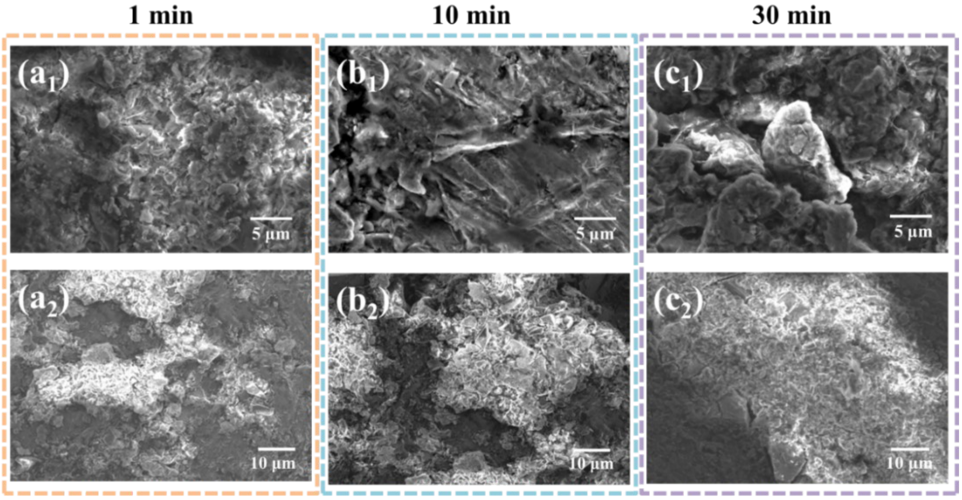

Figure S7. SEM images of the bare zinc anode plating at 0.5 mA cm^{-2} with different time of (a$_1$, a$_2$) 1 min, (b$_1$, b$_2$) 10 min, and (c$_1$, c$_2$) 30 min. Bumpy and upward well-shaped zinc platelets coupled with irregular micro-/nano-particles agglomerates can be clearly observed when plating different amounts on bare Zn anode from 1 to 30 min. The bare Zn anode displays a rough surface propagation implying an uncontrolled and dendritic zinc growth.

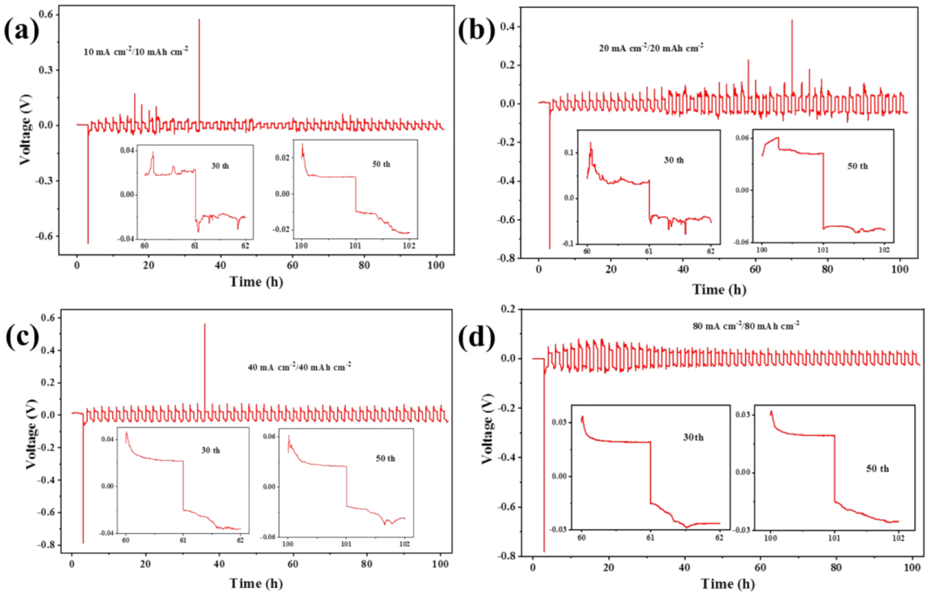

Figure S8. Electrochemical stability tests of bare Sn foil based symmetrical cells at different areal currents/capacities. Cycle performance at (a) 10 mA cm^{-2}/10 mAh cm^{-2}, (b) 20 mA cm^{-2}/20 mAh cm^{-2}, (c) 40 mA cm^{-2}/40 mAh cm^{-2}, and (d) 80 mA cm^{-2}/80 mAh cm^{-2}.

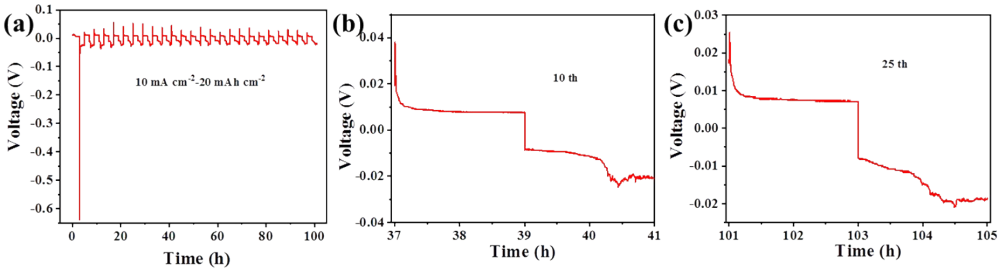

Figure S9. Cycle performance at 10 mA cm^{-2}/20 mAh cm^{-2} of bare Sn foil based symmetrical cells.

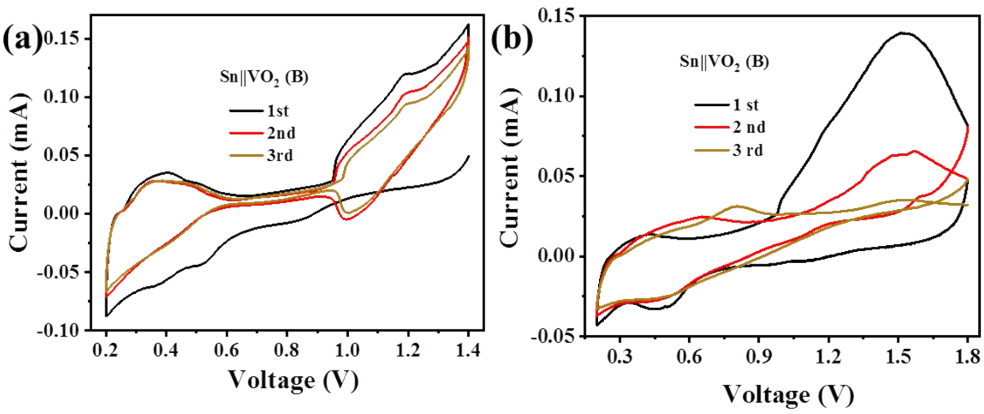

Figure S10. (a, b) The CV curves of Sn foil||VO$_2$(B) full batteries with different voltage ranges at 0.1 mV s^{-1}.

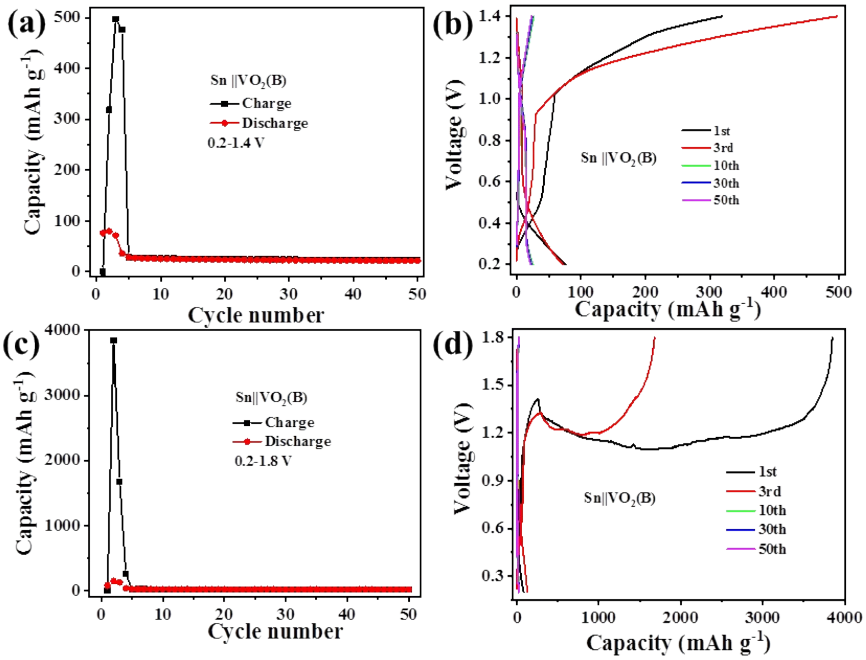

Figure S11. The cycle performance and the corresponding voltage-capacity curves of Sn foil||VO_2(B) full batteries at voltage ranges of (a, b) 0.2-1.4 V and (c, d) 0.2-1.8 V.

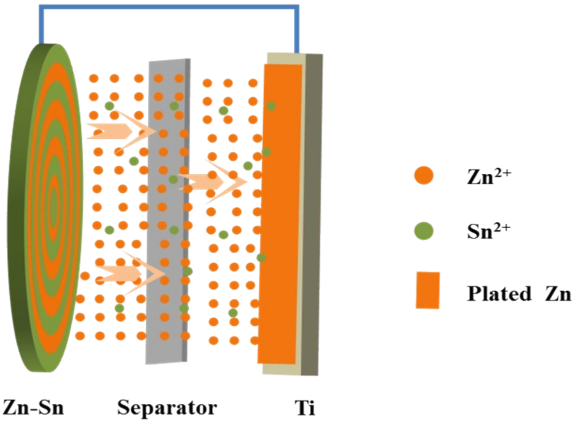

Figure S12. The ion plating schematic of the titanium (Ti) foil||Zn-Sn vertically oriented arrays asymmetrical cell.

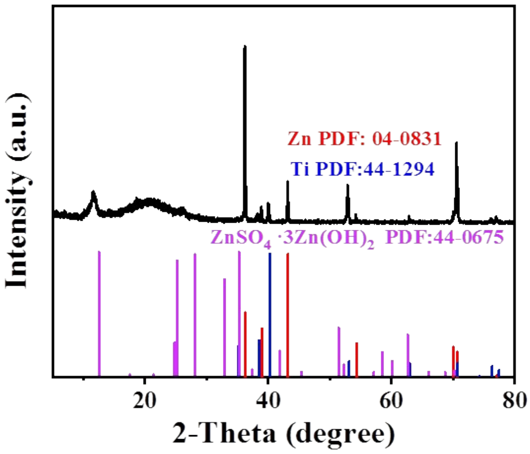

Figure S13. XRD patterns of the plated titanium foil applying the asymmetrical cell in **Figure S12** after the plating process at 0.5 mA cm^{-2}/1 mAh cm^{-2}. It can be seen that the basic zinc sulfate by-product is formed, which is consistent with the previous reports.[1, 2]

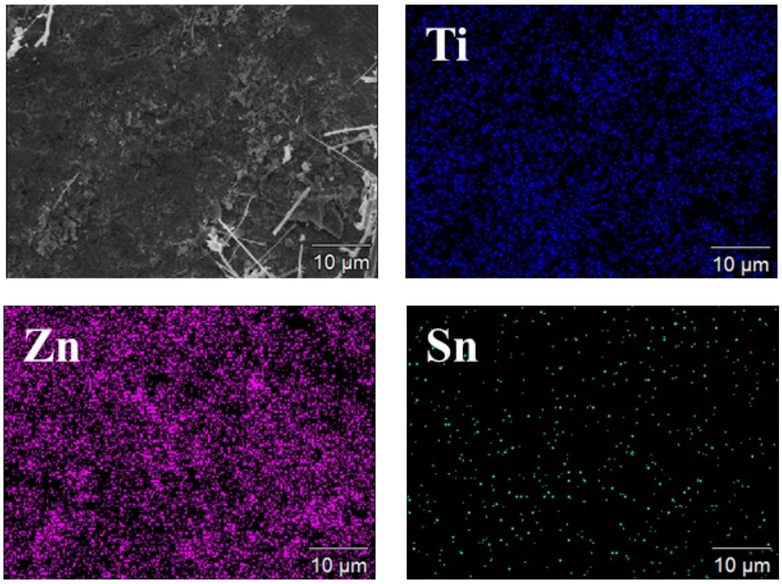

Figure S14. The SEM and the corresponding mapping images of the plated titanium foil applying the asymmetrical cell in **Figure S12** after the plating process at 0.5 mA cm^{-2}/1 mAh cm^{-2}.

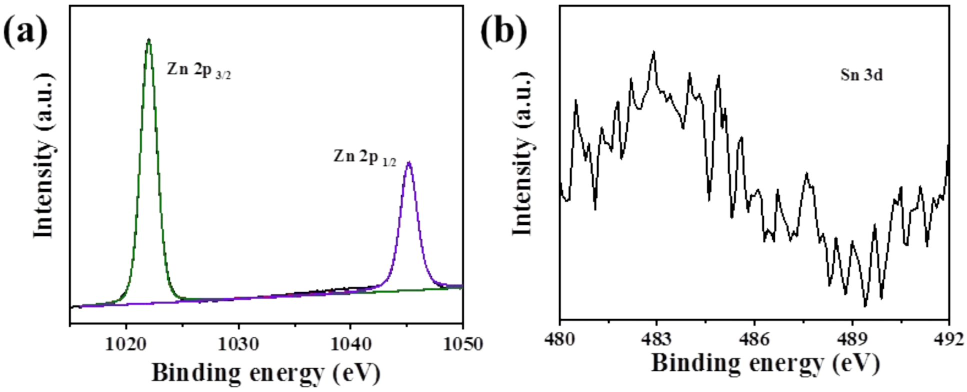

Figure S15. (a, b) XPS spectra of the deposits on Ti surface in the asymmetric cell of **Figure S12** at 0.5 mA cm^{-2}/1 mAh cm^{-2}.

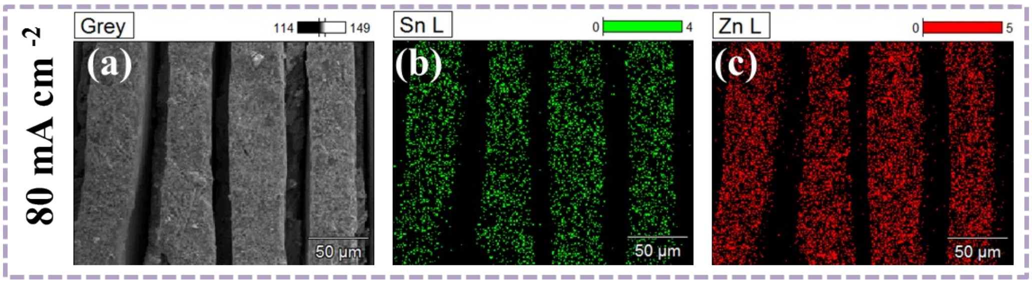

Figure S16. (a-c) The SEM and corresponding mapping images of the Zn-Sn vertical arrays anode after zinc stripping at 80 mA cm^{-2}.

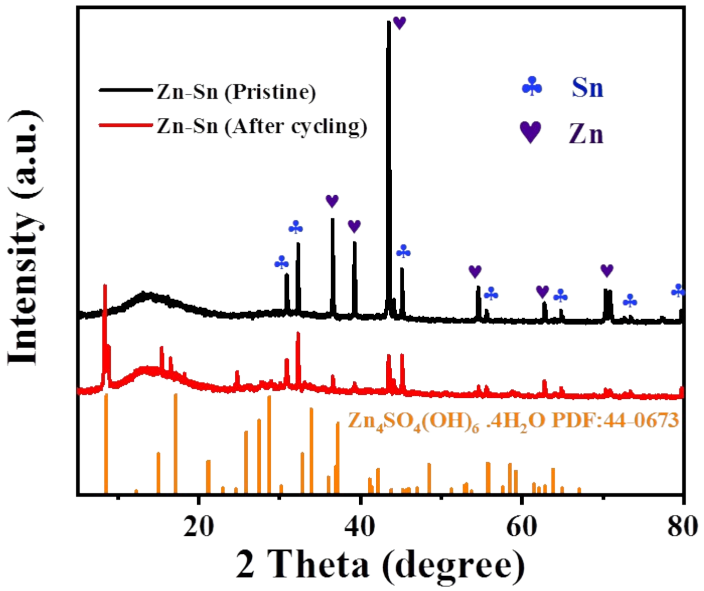

Figure S17. XRD patterns of the Zn-Sn vertical arrays without and with zinc plating/stripping.

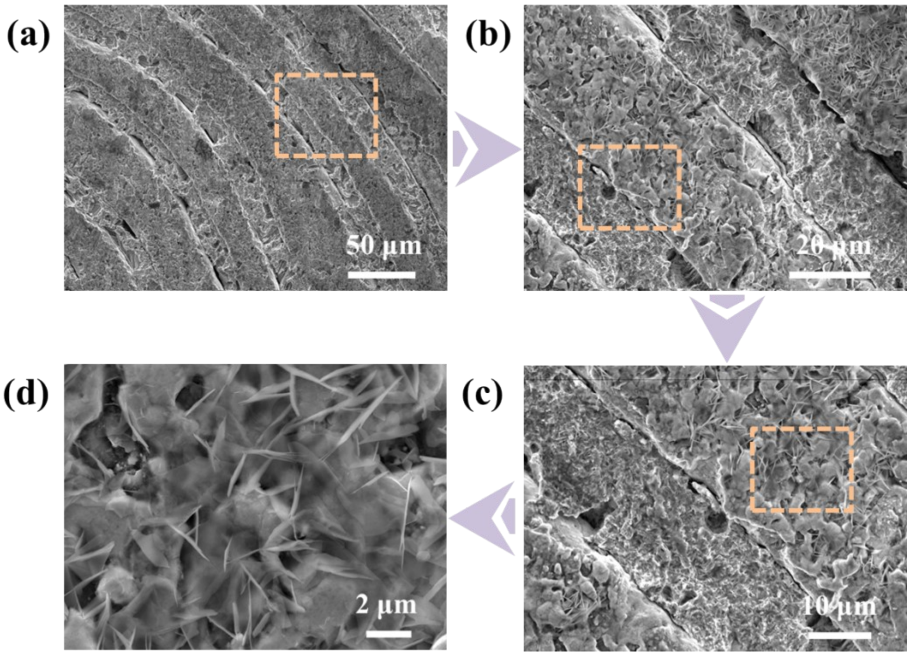

Figure S18. (a-d) SEM images with different magnifications of the Zn-Sn vertical arrays anode after zinc stripping at 20 mA cm^{-2}/2 mAh cm^{-2}.

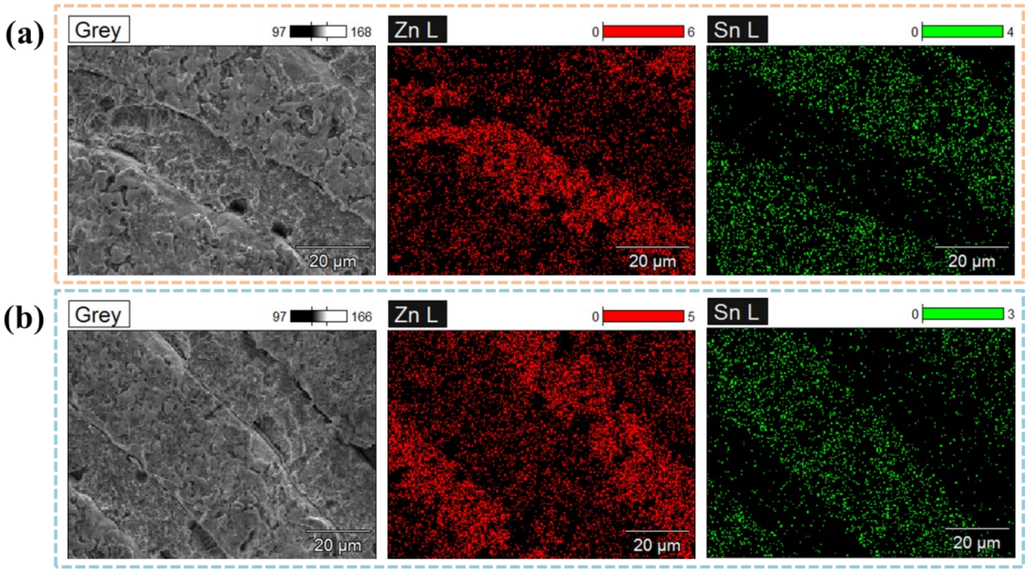

Figure S19. (a, b) The SEM and corresponding mapping images of the Zn-Sn vertical arrays anode after zinc stripping at 20 mA cm^{-2}/2 mAh cm^{-2} at different positions.

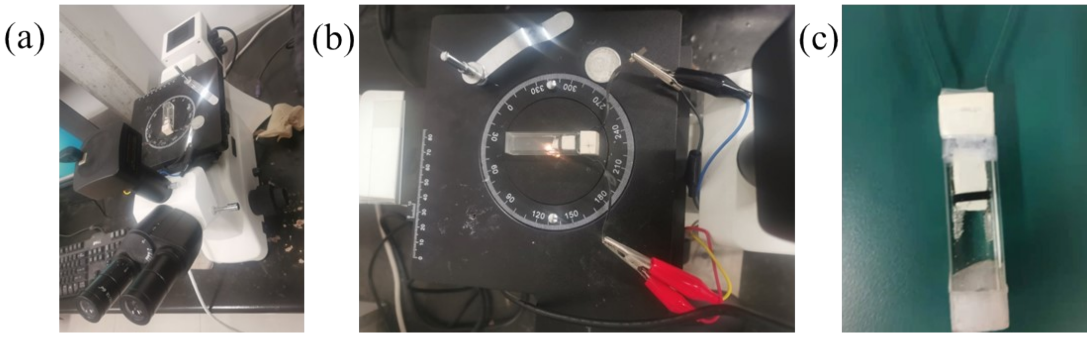

Figure S20. (a-c) Digital images of *in-situ* optical observations and the corresponding test cell.

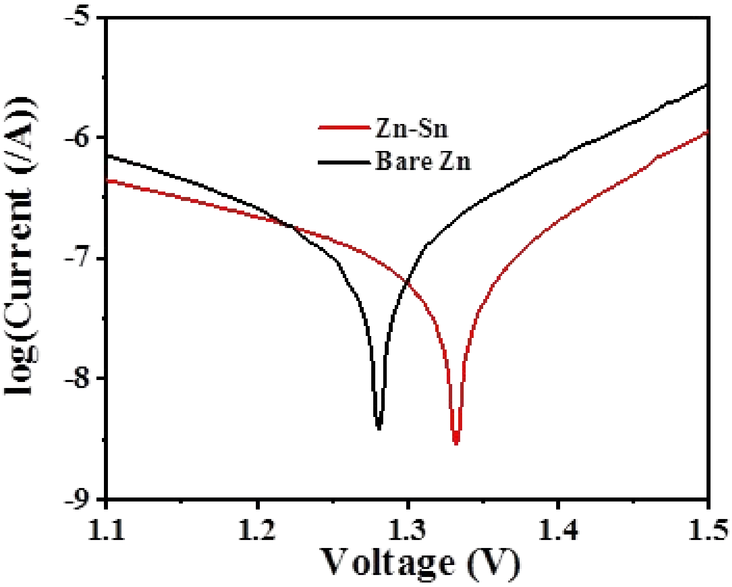

Figure S21. Tafel plots of corrosion behavior for the bare Zn and Zn-Sn vertical arrays anode in 2 M $ZnSO_4$ at the scan rate of 2 mV s^{-1}. The analysis results with different tip potentials of the bare Zn (~1.28 V vs. Zn^{2+}/Zn) and Zn-Sn vertical arrays anode (~1.33 V vs. Zn^{2+}/Zn) indicate that Zn-Sn vertical arrays anode can enhance the corrosion resistance.

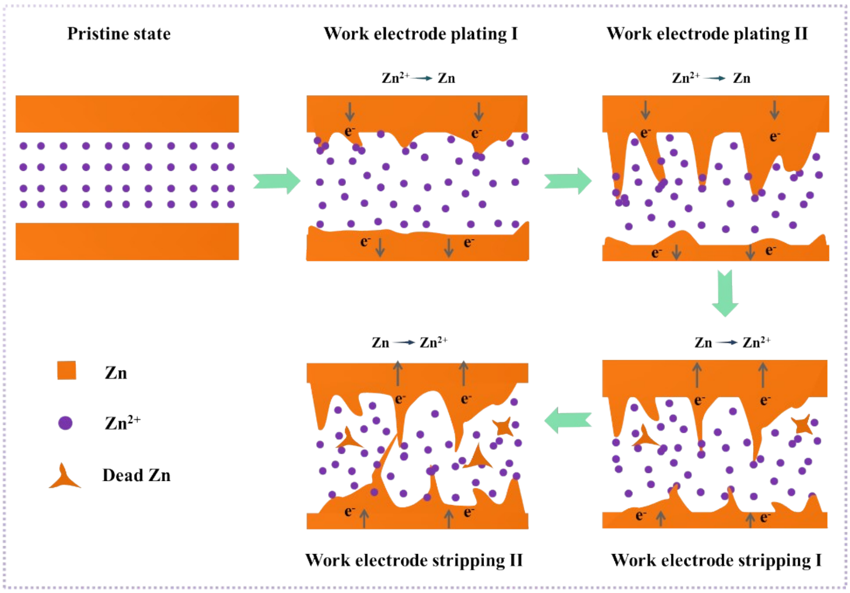

Figure S22. The schematic of the zinc plating/stripping on the bare Zn. Due to the uneven distribution of zinc ions and electric field, zinc dendrites are prone to occur, which can lead to battery failure.

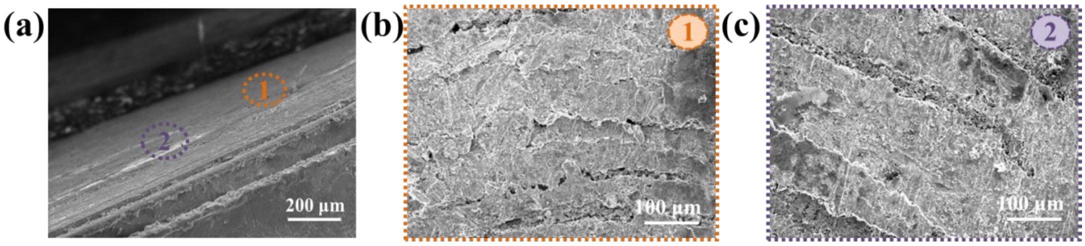

Figure S23. (a-c) Side-view and top-view images of the zinc re-plated Zn-Sn vertical arrays anode.

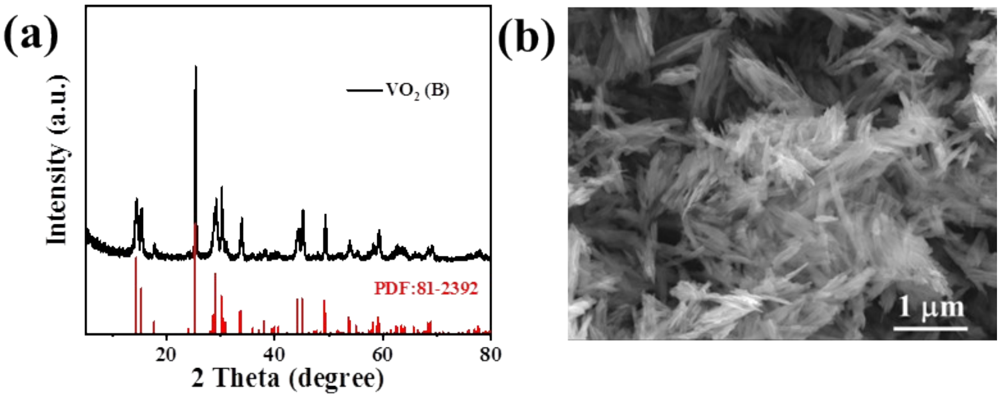

Figure S24. XRD patterns and SEM image of the obtained VO$_2$(B). It can be seen that the main peaks can be indexed to VO$_2$(B) (JCPDS No. 81-2392).

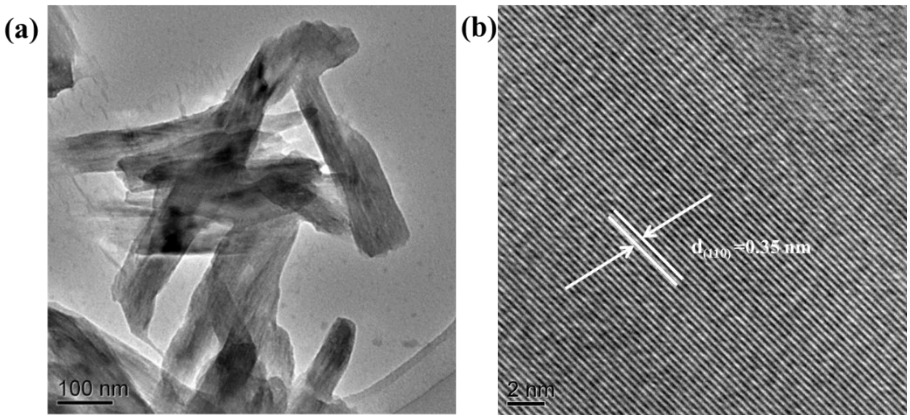

Figure S25. (a, b) Transmission electron microscope images of the obtained VO_2(B) cathode.

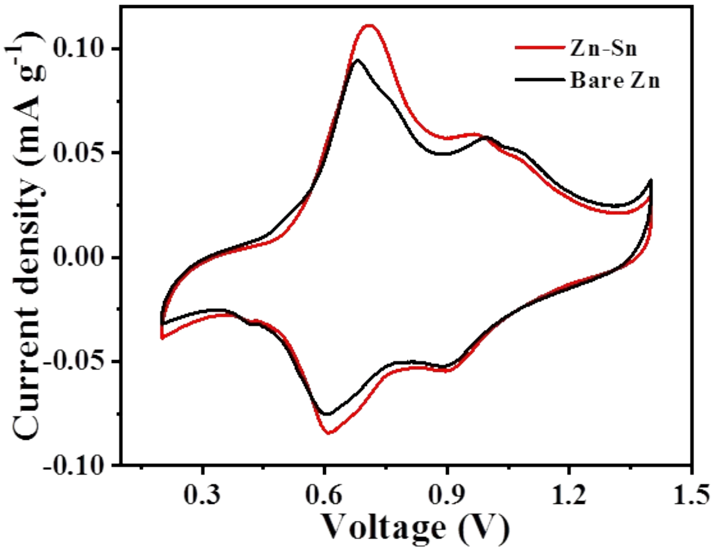

Figure S26. The CV curves of full batteries with the Zn-Sn vertical arrays anode and the bare zinc anode matched with the VO_2(B) cathode at 0.1 mV s^{-1}.

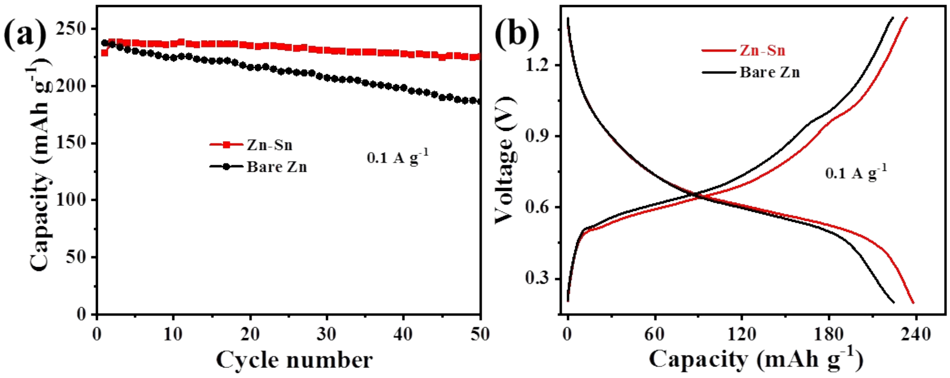

Figure S27. (a) Cycling performance and (b) the corresponding voltage-capacity curves at 1 st.

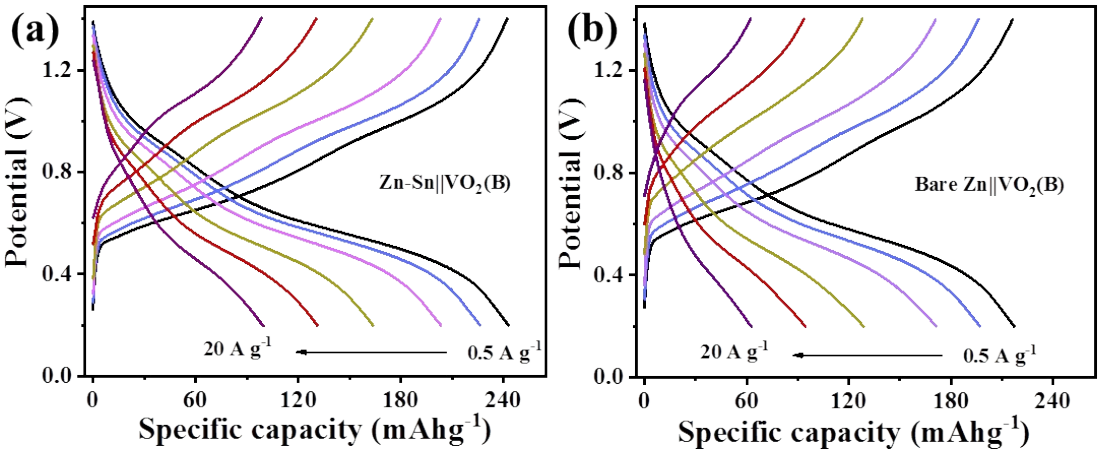

Figure S28. Volage-capacity curves of (a) Zn-Sn||VO_2(B) and (b) bare Zn||VO_2(B) full batteries at different current densities from 0.5, 1, 2, 5, 10 to 20 A g^{-1}.

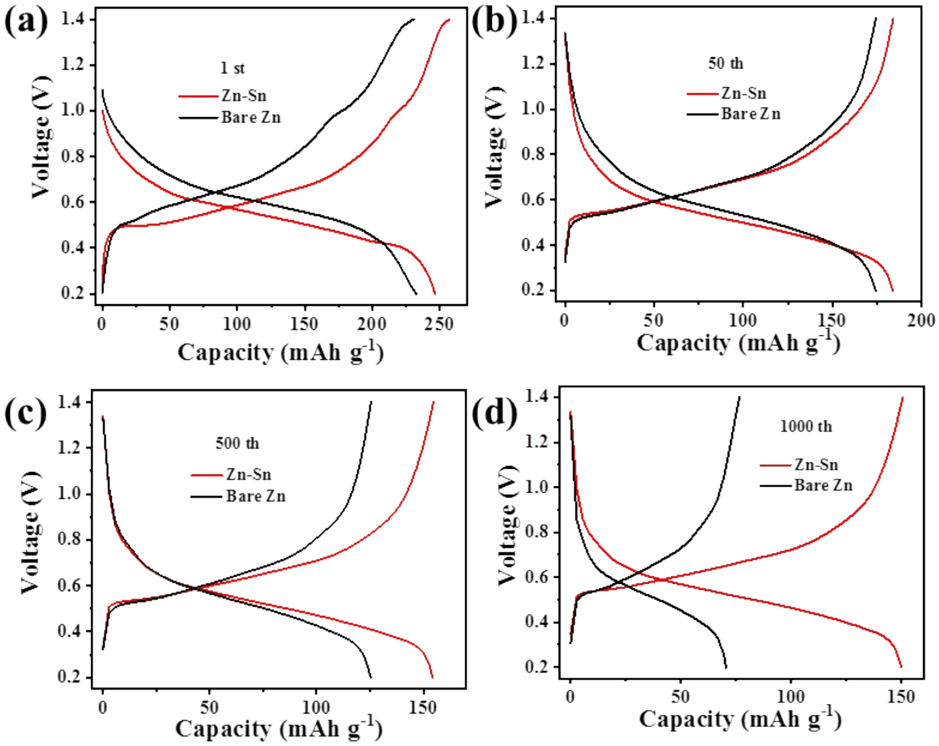

Figure S29. (a-d) Volage-capacity curves of Zn-Sn||VO_2(B) and bare Zn||VO_2(B) full batteries at different cycle times. The batteries were activated for 3 cycles at 0.1 A g^{-1}, and then cycled at 2 A g^{-1}.

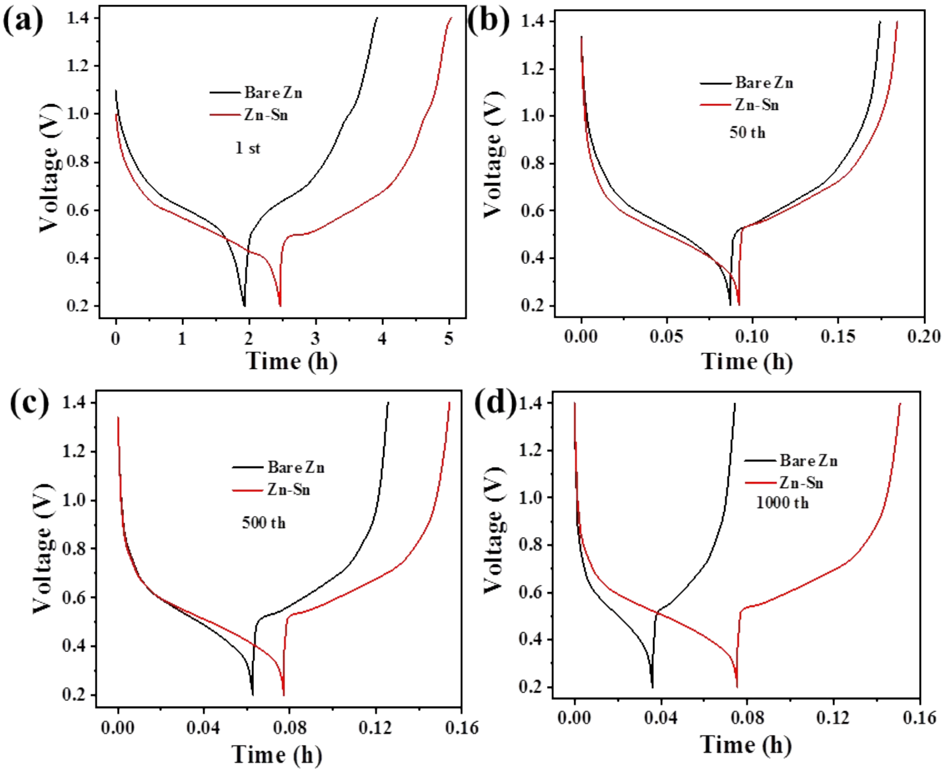

Figure S30. (a-d) Volage-time curves of Zn-Sn||VO$_2$(B) and bare Zn||VO$_2$(B) full batteries at different cycle times. The batteries were activated for 3 cycles at 0.1 A g^{-1}, and then cycled at 2 A g^{-1}.

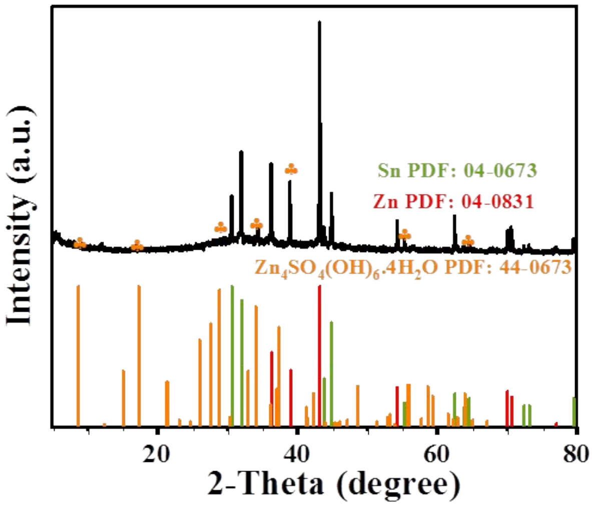

Figure S31. XRD patterns of the Zn-Sn vertical arrays anode of the Zn-Sn||VO_2(B) full battery after zinc plating/stripping. It can be seen that there are without side reactions. Of note, the formation of basic zinc sulfate by-product is inevitable for applying zinc sulfate electrolyte.[1, 2]

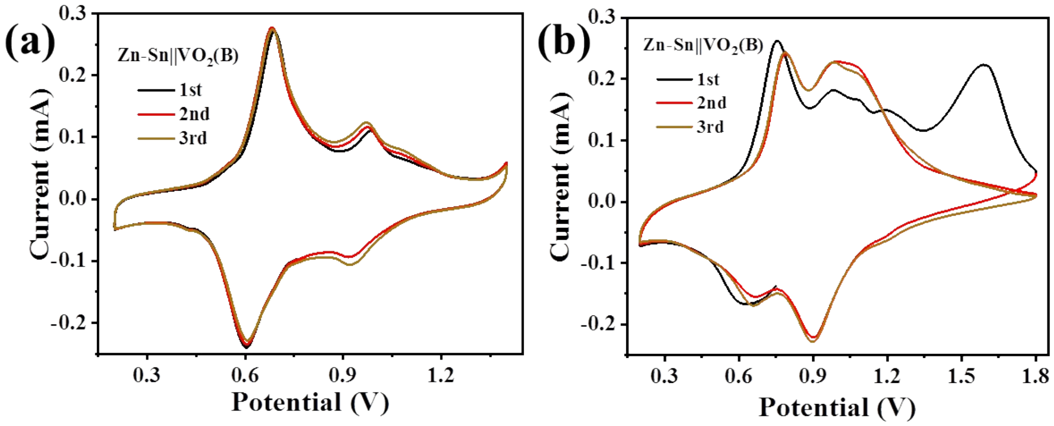

Figure S32. (a, b) The CV curves of Zn-Sn vertically oriented arrays anode||VO_2(B) full batteries with different voltage ranges at 0.1 mV s^{-1}. The peaks of CVs belong to the electrochemical behavior of the VO_2(B) cathode. For the VO_2(B) cathode, the zinc ion storage mechanisms are totally different via applying the low (not higher than 1.5 V vs. Zn^{2+}/Zn) and high (>1.5 V vs. Zn^{2+}/Zn) charging voltages. For CVs with the voltage range of 0.2-1.4 V, two pairs redox peaks correspond to two-step zinc ion storage reactions.[3, 4] When charging voltage is about 1.6 V, there will be an irreversible phase transition process of the VO_2(B) cathode. The subsequent redox peaks are belonged to the zinc storage processes of the obtained new-phase product such as V_2O_5 or $Zn_3(OH)_2V_2O_7{\cdot}2H_2O$.[5, 6]

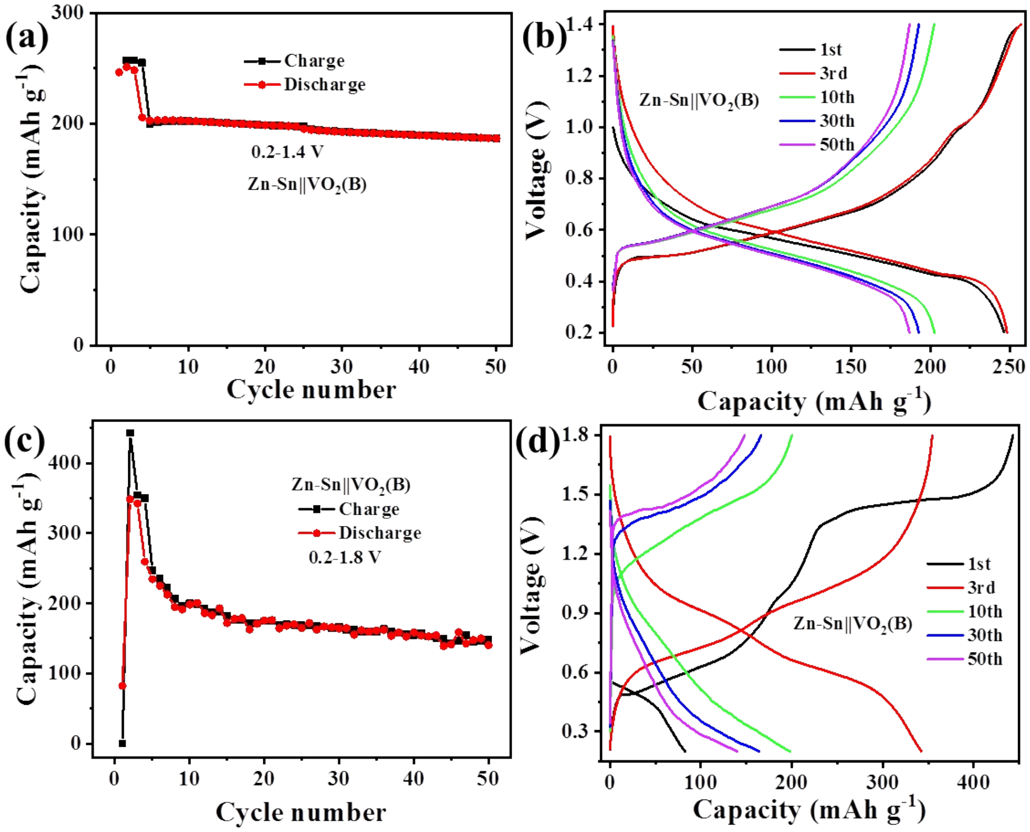

Figure S33. The cycle performance and the corresponding voltage-capacity curves of Zn-Sn vertically oriented arrays anode||VO_2(B) full batteries at different voltage ranges of (a, b) 0.2-1.4 V and (c, d) 0.2-1.8 V. All batteries were cycled 3 times at 0.1 A g^{-1}, and then cycled to 50 times at 2 A g^{-1}.

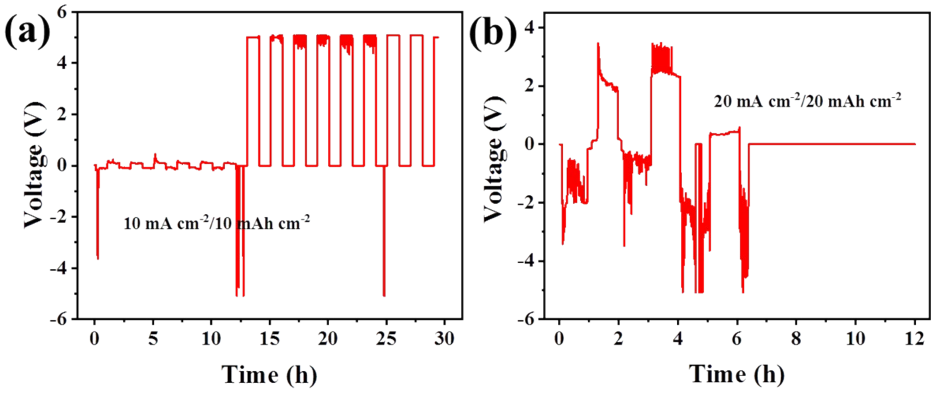

Figure S34. The electrochemical performance of the Zn-Sn vertically oriented arrays based symmetrical batteries with the ZnO saturated 6 M KOH electrolyte. Cycle performance at (a) 10 mA cm^{-2}/10 mAh cm^{-2} and (b) 20 mA cm^{-2}/20 mAh cm^{-2}.

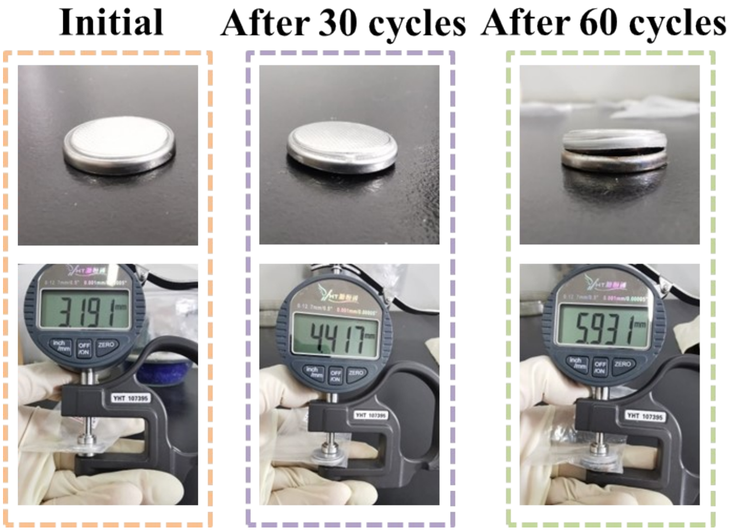

Figure S35. Optical images of Zn-Sn vertically oriented arrays||$Ni(OH)_2$ full batteries at different situations.

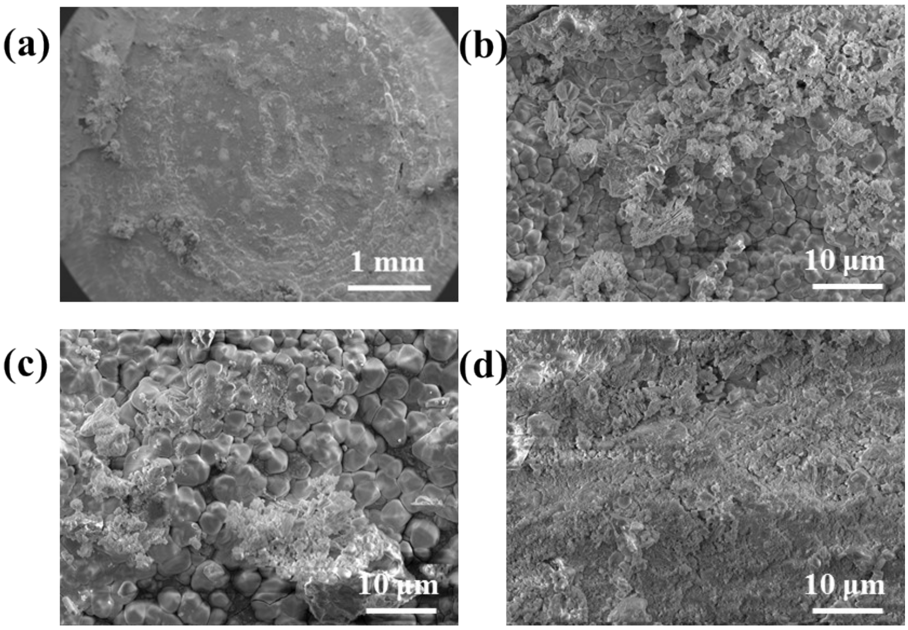

Figure S36. (a-d) SEM images at various areas of the cycled Zn-Sn vertical arrays anode of Zn-Sn vertically oriented arrays||Ni$(OH)_2$ full batteries.

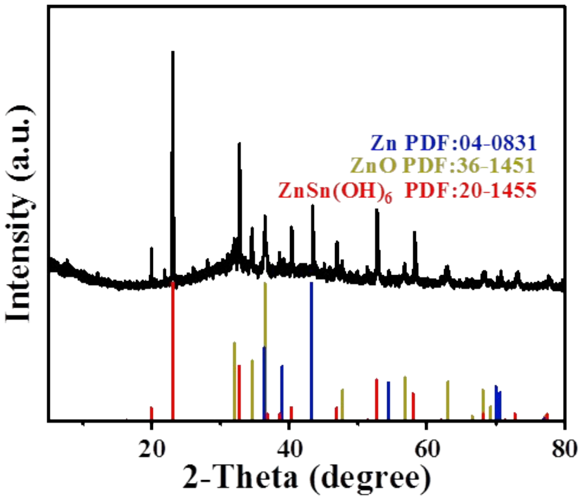

Figure S37. XRD patterns of the cycled Zn-Sn vertical arrays anode of Zn-Sn vertically oriented arrays||$Ni(OH)_2$ full batteries.

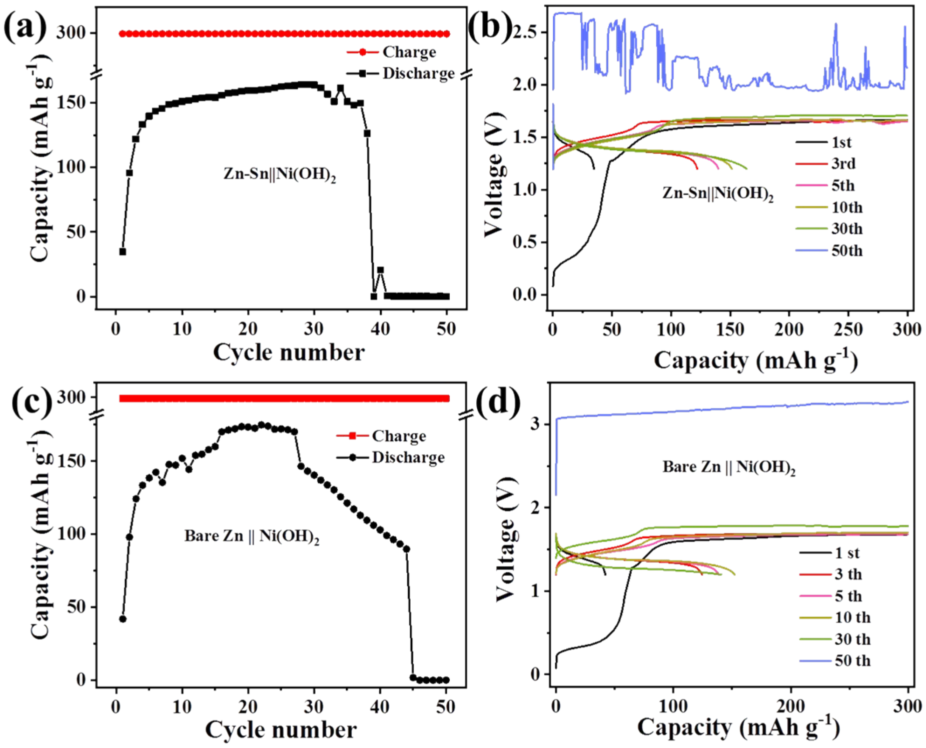

Figure S38. (a-d) The electrochemical performance of the Zn-Sn vertically oriented arrays||$Ni(OH)_2$ and the pure zinc foil||$Ni(OH)_2$ full batteries. (a, c) The cycle stability and (b, d) the corresponding voltage-capacity profiles. The battery test conditions are: charge for 0.5 h at 2 C, and discharge to 1.2 V at 2 C (1 C =300 mAh g^{-1}). The battery capacity is based on $Ni(OH)_2$.

Table S1 ICP-OES data of the deposits on Ti foil in asymmetric cell of **Figure S12** at 0.5 mA cm^{-2}/1 mAh cm^{-2}.

ICP-OES data	**Zn**	**Sn**
Sample-1	38.13 mg L^{-1}	0.12 mg L^{-1}
Sample-2	38.16 mg L^{-1}	0.14 mg L^{-1}
Sample-3	38.18 mg L^{-1}	0.17 mg L^{-1}
Average value	38.16 mg L^{-1}	0.14 mg L^{-1}
Average mass ratio	272.57	1.00
Average mole ratio	499.02	1.00
Mole percentage of Sn	0.20 %	

Reference

1. C. Wang, S. Wei, S. Chen, D. Cao and L. Song, *Small Methods*, 2019, **3**, 1900495.
2. L. Ma, Q. Li, Y. Ying, F. Ma, S. Chen, Y. Li, H. Huang and C. Zhi, *Adv. Mater.*, 2021, **33**, 2007406.
3. N. Liu, X. Wu, L. Fan, S. Gong, Z. Guo, A. Chen, C. Zhao, Y. Mao, N. Zhang and K. Sun, *Adv. Mater.,* 2020, **32**, 1908420.
4. J. Ding, Z. Du, L. Gu, B. Li, L. Wang, S. Wang, Y. Gong and S. Yang, *Adv. Mater.,* 2018, **30**, 1800762.
5. T. Wei, Q. Li, G. Yang and C. Wang, *J. Mater. Chem. A*, 2018, **6**, 8006-8012.
6. J. Ding, H. Gao, K. Zhao, H. Zheng, H. Zhang, L. Han, S. Wang, S. Wu, S. Fang and F. Cheng, *J. Power Sources*, 2021, **487**, 229369.